Key Engineering Materials
ISSN: 1662-9795, Vol. 988, pp 31-46
doi:10.4028/p-G6Pyxv

Submitted: 2023-08-08
Revised: 2024-03-04
Accepted: 2024-03-06
Online: 2024-09-27

A Modelling Framework for Rapid Evaluation of Speed Limitations During Extrusion of Aluminium Profiles

Mads Iddberg[1,a*], Ole Runar Myhr[2,3,b], Anders Nesse[4,c] and Trond Furu[5,6,d]

[1]SINTEF Manufacturing, Raufoss, Norway

[2]Hydro Aluminium R&D, Sunndalsøra, Norway

[3]NTNU, Department of Structural Engineering, Trondheim, Norway

[4]Hydro Extrusions, Oslo, Norway

[5]Norsk Hydro, Corporate Technology Office, Oslo, Norway

[6]NTNU, Department of Material Science and Engineering, Trondheim, Norway

[a]mads.iddberg@sintef.no, [b]ole.runar.myhr@hydro.com, [c]anders.nesse@hydro.com, [d]trond.furu@hydro.com

Keywords: Extrusion simulations, Temperature models, Extrusion speed, 6xxx alloys.

Abstract. Hot tearing is a well-known limitation when trying to maximize the throughput rate in aluminium extrusion. In the present work an analytical modelling framework is presented which can be used to predict the maximum extrusion speed that can be applied in production without formation of this type of surface defect. The modelling framework allows almost instantaneous estimates on the resulting productivity in terms of maximum extrusion speed. This is obtained by developing an analytical model for the maximum temperature at the die exit which incorporate the effect of alloy composition and billet processing. The results are consolidated into extrusion limit diagrams, mapping the maximum allowable extrusion speed as a function of billet pre-heat temperature, alloy composition, and homogenisation heat treatment. The calculated temperatures and extrusion limit diagrams obtained from the analytical model are compared with measured temperatures and critical extrusion speeds from extrusion tests of various 6xxx series alloys for a simple rod-shaped geometry. The comparisons indicate that the presented modelling approach gives sufficiently accurate predictions for future application in optimisation of alloy composition and process parameters in extrusion of profiles.

Introduction

In the production of aluminium extrusions, it is crucial to closely control the surface temperature of the profile at the die exit in order to prevent surface defects [1-3]. This quality requirement must be met while also striving for high extrusion speeds to minimize production costs. Today, this delicate balance between profile quality and productivity is increasingly guided by computer simulations utilizing commercially available FEM codes. Even though these numerical tools are highly sophisticated and can account for detailed behaviour in extrusion equipment and material flow, the relatively high computational time makes them unsuited for rapid evaluation of the combined effect of changes in multiple process parameters. From a productivity point of view, the question is what selection of parameters yield the highest profile throughput. This question can not be answered by a single FEM simulation, which only provides results from one combination of process parameters. In contrast, analytical models allow almost instantaneous estimates of the parameters evaluated, making them well suited to map the connection between the process parameters yielding maximum productivity.

A main objective of the present work is to create a model capable of predicting the effect of different alloy compositions and heat treatment schedules on the resulting maximum temperature of the profile at the die outlet. The model is tested against experimental data as well as compared to predictions made with the commercially available software HyperXtrude®[4]. To establish the extrusion limitations, it requires that the hot-deformation resistance of the alloy can be estimated and

included in the constitutive equations of the models. The hot-deformation resistance, defined as the effective flow stress in compression, differs significantly at different positions of the billet and profile as it depends on the instantaneous values of strain rate and temperature, as well as the instantaneous state of the microstructure. For 6xxx series alloys containing dispersoids, it has been shown that these particles increase the deformation resistance significantly [5,6]. Hence, two billets with identical alloy composition may give different hot-deformation resistance if they have been homogenised at different temperatures. This is because the resulting dispersoid size distribution depends on the homogenisation temperature, and because the deformation resistance increases with increasing number density of dispersoids. The relationship between homogenisation cycle, dispersoid density, and resulting hot-deformation resistance has important practical implications, since an alloy with a high hot-deformation resistance cannot be extruded as fast as an alloy with low hot-deformation resistance when surface defects are to be avoided. In the present work, the microstructure model Alstruc [7,8], which will be briefly described below, has been used to predict the resulting dispersoid levels after casting and homogenisation for the various alloys considered.

While the first part of the article deals with predictions of temperatures, the second part utilizes the calculated temperatures to establish extrusion limit diagrams. Different types of surface defects may form during extrusion, like die lines, pick-up and hot tearing [1-3]. In the present work, hot tearing is assumed to be the critical surface defect which determines the maximum allowable extrusion speed. Hot tearing is usually attributed to two different types of mechanisms [2,3,9], i.e. tearing that occurs when the aluminium matrix can no longer withstand the frictional forces of the die, or tearing caused by incipient melting of particles close to the surface. Both tearing mechanisms are associated with critical temperatures that are alloy specific and can be estimated from phase-diagrams [2,3,9].

The calculated temperatures and the calculated extrusion limit diagrams are validated by comparing predictions with a comprehensive experimental database containing measurements of the die exit temperatures and corresponding data for the transition from acceptable surface appearance to surface tearing. These comparisons indicate that the presented modelling approach gives sufficiently accurate predictions for future application in optimisation of process parameters in extrusion of aluminium profiles.

Theory

The different models used in the present work are outlined below. The microstructure model and the FEM-model are both just briefly described since details of the underlying theory and assumptions are given in the references. The theoretical background for the analytical model is described in more details since this model has not been published previously.

Microstructure Model. The microstructure-based simulation model Alstruc [7,8] is used to predict important microstructure parameters for the alloys. The program predicts the formation of dispersoids that may precipitate from solid solution during the homogenisation cycle if the alloy contains elements like Mn or Cr, and the resulting mean concentration of elements in solid solution. The required inputs to this model include chemical composition, the local solidification rate during casting, and the complete homogenisation cycle. Other outputs from the model, which are not used in the present work, include the volume fraction and size distributions of coarse primary particles, and the local variations of alloying elements (i.e. microsegregation) across a representative dendrite arm.

FEM Model. The extrusion process is simulated using HyperXtrude®[4], which is a commercially available FEM software. In this work, the software is used to calculate the temperature at the surface of the profile at the die exit, assuming steady state conditions and rigid tool surfaces. The simulation requires a description of the flow stress in the material, which in the present work is modelled by a modified Sellars-Tegart relationship, Eq. 3, described in more detail in [6,10]. This relationship predicts the flow stress in a material point as a function of strain rate, temperature, and the initial state of the microstructure in the billet. The friction at the bearing region is described with a viscoplastic relation [4], applying a friction coefficient of 0.3. All other contact between the solid boundary and

the flow domain is modelled with the Dirichlet boundary condition. The FEM predicted exit temperatures are compared to the experimentally obtained data both as a verification of the implemented material model and as a reference for the results obtained with the analytical model.

Analytical Model. The analytical model is based on the simplified assumption of independent temperature contributions that are added linearly similar to the approach used in several previous developed models [11-14]. The profile surface temperature T_s at the die exit at steady state conditions can then be expressed as follows:

$$T_s=T_0+\sum_i \Delta T_i. \quad (1)$$

Here, T_0 is the initial billet temperature, and ΔT_i is the specific temperature increase from mechanism i. Eq. 1 assumes that the individual contributions to the temperature increase are mutually independent, which is obviously a simplification. The use of Eq. 1 as a basis for temperature predictions is justified by comparing temperatures obtained from this equation with temperature measurements and more accurate predictions obtained by finite element simulations. In the following, the different contributions ΔT_i in Eq. 1 are explained in more details.

Adiabatic Heating. The first contribution, i.e. ΔT_1, is the temperature increase caused by the work of deformation that is almost entirely converted into heat (i.e. adiabatic heating). This contribution can be expressed as follows [15]:

$$\Delta T_1=\beta \frac{\bar{\sigma} \ln(R)}{\rho c}. \quad (2)$$

Here, β represents an efficiency in terms of the fraction of the deformation work that is converted to heat. $\bar{\sigma}$ is the effective flow stress, R is the reduction ratio, and ρ and c are the density and the specific heat capacity of the alloy, respectively. This idealised heating does not account for "redundant work", which according to Dieter [15] is "work involved in internal shearing processes due to non-uniform deformation that does not contribute to the change in the shape of the body". Neither does ΔT_1 account for heat generation due to friction.

It follows from Eq. 2 that ΔT_1 is proportional to the mean equivalent stress $\bar{\sigma}$. As shown in Refs. [6,10], the following version of the Sellars-Tegart relationship has been demonstrated to give good agreement with hot-deformation tests for a range of different 6xxx series alloys:

$$\bar{\sigma}=\sigma_{ss} \operatorname{arcsinh}\left(\frac{ZH}{C}\right)^{1/n}+\sigma_d. \quad (3)$$

Here, σ_{ss} and σ_d are material constants which describe the deformation resistance of the alloy. C and n are material constants with values set to 7.0 x 10^8 s^{-1}, 5.0 and 156 kJ/mol, respectively [6,10]. ZH is the Zener-Hollomon parameter defined as:

$$ZH=\dot{\varepsilon} \exp\left(\frac{Q_{app}}{R_g T_{def}}\right). \quad (4)$$

Here, $\dot{\varepsilon}$, Q_{app}, R_g, and T_{def} are the strain rate, the apparent activation energy, the universal gas constant, and the deformation temperature, respectively. For Q_{app}, the common value of 156 kJ/mol has been applied in the simulations. $\bar{\dot{\varepsilon}}$ in Eq. 5 is estimated as the effective strain rate defined by the time for material to transverse through a truncated conical volume of deformation zone defined by the container diameter D_c, the extrusion diameter D_e, and the semi-die angle α_d. For a ram speed v_r, we get [16]:

$$\bar{\dot{\varepsilon}}=\frac{6 v_r D_c^2 \ln R \tan \alpha_d}{D_c^3-D_e^3}. \quad (5)$$

In Eq. 3, σ_{ss} and σ_d are material constants which can be attributed to the deformation resistance from elements in solid solution and from non-shearable particles, respectively. σ_{ss} depends on the solid solution concentrations of the alloy and is expressed by an overall concentration parameter C_{ss} as follows [6,10]:

$$\sigma_{ss}=k_{ss}C_{ss}^{3/4}. \tag{6}$$

Here, k_{ss} is a constant equal to 3.0MPa $(wt\%)^{-3/4}$ [6,10]. σ_d in Eq. 3 can be estimated from the number density and size of the dispersoids that have formed during homogenisation according to the following relationship [6,10]:

$$\sigma_d=k_d\sqrt{N_d r_d}\ . \tag{7}$$

In this equation, k_d is a constant equal to 4.8MPa (m^{-1}) [6,10], and N_d and r_d are the number density and average radius of the dispersoids, respectively.

The temperature increase ΔT_1 can now be calculated by combining Eqs. 3-7. When the deformation temperature T_{def} is approximated by the initial billet temperature T_0, we get:

$$\bar{\sigma}=k_{ss}C_{ss}^{3/4}\operatorname{arcsinh}\left(\left(\frac{6v_rD_c^2\ln(R)\tan(\alpha_d)}{C\left(D_c^3-D_e^3\right)}\exp\left(\frac{Q_{app}}{RT_0}\right)\right)^{1/n}\right)+k_d\sqrt{N_d r_d}. \tag{8}$$

From Eq. 8, the effective flow stress $\bar{\sigma}$ can be calculated as a function of geometric dimensions (i.e. D_c, D_e, and $R=D_c^2/D_e^2$), extrusion process parameters as given by the initial billet pre-heat temperature T_B and the ram speed v_r, as well as the material parameters C_{ss}, N_d, and r_d. These material parameters are obtained from the Alstruc-model and represent the link between the casting and homogenisation processes, and the extrusion process in the present temperature model.

Heat Generation Due to Friction Between Profile and Die. Friction between the deforming profile and the bearing surface in the die channel leads to heat generation. In parts of the bearing surface, sticking friction may be prominent while sliding friction may occur in other parts of the bearing surface [17]. In the present model, this temperature increase has been calculated as follows:

$$\Delta T_2=\frac{\bar{\sigma}}{4\sqrt{3}\rho c}\sqrt{\frac{v_eL_d}{\alpha}} \quad \text{when} \quad d>2\sqrt{\alpha\frac{L_d}{v_e}}\ . \tag{9a}$$

$$\Delta T_2=\frac{\bar{\sigma}}{4\sqrt{3}\rho c}\sqrt{\frac{2L_d}{d}} \quad \text{when} \quad d\le 2\sqrt{\alpha\frac{L_d}{v_e}}\ . \tag{9b}$$

Here, v_e, is the extrusion speed equal to v_rR, where R is the reduction ratio. L_d is the bearing length of the die and α is the thermal diffusivity of the material equal to $\lambda/(\rho c)$. Eq. 9a is derived by assuming that the heat generation due to friction between the die and the profile gives a temperature increase in a surface shell with a thickness corresponding to an estimated diffusion length $\sqrt{\alpha t}$, where the time t can be approximated by L_d/v_e [11]. When the diffusion length exceeds the die bearing channel thickness, i.e. the profile thickness d, the generated heat is assumed to contribute to an increase in the temperature in the whole thickness, as expressed by Eq. 9b. Eq. 9a and Eq. 9b assume heat generation along the whole bearing length L_d. If this is not the case, L_d must be replaced by an efficient bearing length which corresponds to the estimated length where the friction is strong enough to cause significant heating.

Heat Generation Due to Friction Between Container and Billet. There will be a temperature increase at the billet surface caused by friction between the container wall and the billet surface, which can be estimated as follows [11]:

$$\Delta T_3=\frac{\bar{\sigma}}{4\sqrt{3}\rho c}\sqrt{\frac{v_r L_b}{\alpha}}\,. \tag{10}$$

Here, L_b is the billet length. The equation is derived by assuming that the heat developed by friction is divided equally and uniformly between the billet and the container to a depth that is estimated as $\sqrt{\alpha t}$ where t is approximated as L_b/v_r [11].

Heat Conduction in Container and Billet. Usually, there is an initial temperature difference between the billet and the container. Since the heat transfer coefficient between the billet surface and the container wall is deemed to be high when the extrusion starts, it may be reasonable to assume that there is a common interface temperature T_{int} between billet and container. It can be shown that T_{int} does not vary significantly during an initial time period [18], which allows the temperature in the billet at a distance *x* from the billet surface at time *t*, T(x,t) to be calculated as follows [18]:

$$T(x,t)=T_{int}+(T_0-T_{int})\,\mathrm{erf}\left(\frac{x}{2\sqrt{\alpha t}}\right). \tag{11}$$

Here, T_{int} and T_0 are the temperature at the interface between the aluminium billet and the steel container, and the initial billet temperature, respectively, and erf is the error function. Similarly, as for the prediction of ΔT_3, the conduction in the billet is assumed to be one dimensional, which is a reasonable approximation for large cylinder diameters. The interface temperature T_{int} can be estimated as follows [18]:

$$T_{int}=\frac{T_0\sqrt{\lambda\rho c}+T_c^0\sqrt{\lambda_c\rho_c c_c}}{\sqrt{\lambda\rho c}+\sqrt{\lambda_c\rho_c c_c}}\,. \tag{12}$$

Here, T_c^0 is the initial temperature of the container. λ , ρ, and c, are thermal conductivity, density, and specific heat capacity, respectively, and index c refers to the container. The thermal diffusion distance x can be approximated as follows:

$$x=k_4\sqrt{\alpha t}. \tag{13}$$

Here, k_4 is a dimensionless constant, which depends on the temperature considered. In the present work, a best fit value of 0.55 was used in the model. By combining Eq. 11 and Eq. 13, we get the following expression for the billet temperature at a distance *x* from the billet surface at time t:

$$T_b=T_{int}+(T_0-T_{int})\,\mathrm{erf}(k_4/2). \tag{14}$$

Finally, we define ΔT_4 as the difference between the actual billet temperature and the initial billet temperature as follows:

$$\Delta T_4=T_b-T_0. \tag{15}$$

By combining Eq. 14 and Eq. 15, we get:

$$\Delta T_4=(T_{int}-T_0)\left(1-\mathrm{erf}(k_4/2)\right). \tag{16}$$

Here, T_{int} is given in Eq. 12. Note that ΔT_4 is negative when the initial container temperature is lower than the initial billet temperature, which is usually the case in practice.

Heating due to redundant work. The equations above describing the different contributions to the temperature increase, are highly idealised. In addition, the so-called redundant work has not been accounted for. According to Dieter [15], the redundant work is the work involved in internal shearing processes due to non-uniform deformation that does not contribute to the change in the shape of the body. Redundant work includes the heat generation due to friction between the flowing metal and the stationary metal in the dead-metal zone. According to Saha [19], this heat generation scales with the effective flow stress $\bar{\sigma}$ and the local material speed at the given position. Hence, it is reasonable to

assume that the contribution to temperature increases due to redundant work, i.e. ΔT_5, also scales with the same parameters. If we approximate the local material speed to the ram speed, we get:

$$\Delta T_5 = k_5 v_r \bar{\sigma} . \quad (17)$$

In this expression, the constant k_5 is expected to depend on several geometrical parameters including the reduction ratio R. In the present work, k_5 was calibrated, and a best fit value of 8.0×10^{-8} $Kms(N)^{-1}$ was used for all temperature calculations.

Experimental Data

The experimental data used for validation of the predictive power of the model is a dataset containing results for extrusion of a solid rod, extruded with eight different 6xxx series alloys, reported in [5, 20]. Included in this work is experimental results of a total of 207 unique combinations of alloy composition, homogenisation cycle, billet preheat temperatures and ram speeds. For each experiment the temperature was measured at the die exit and the surface quality was categorised in one of the three categories: no tearing, incipient tearing or tearing. For each combination of alloy and homogenisation cycle, the experiments were conducted by increasing the ram speed for relatively constant values of billet preheat temperature until tearing occurred. The approximate levels of billet preheat temperature tested was 420 °C, 460 °C and 500 °C. The minimum ram speed for all billet preheat temperatures was 4 mm/s, but the maximum ram speed tested varied with the ability of the material to withstand tearing.

Alloy Composition and Homogenisation Cycles. Cylindrical ingots with 95 mm diameter were direct chill cast to approximately 1.8 m lengths and cut into 200 mm billet lengths for extrusion tests. The alloy composition is given in Table 1. Two different homogenisation cycles were used for each alloy composition. The first homogenisation cycle consisted of six hours heating time, followed by soaking at 575 °C for two hours before cooling at a rate of 400°C/hour. The second homogenisation cycle consisted of four hours heating time, followed by soaking at 530 °C for two hours before cooling at a rate of 550 °C/hour. [5, 20]. The former homogenisation cycle was given index "1", and the latter "2". In the article, the combination of alloy composition and homogenisation cycle is referred to as for instance A1, which means alloy composition A, and homogenisation cycle 1. All experimental data, with the exception of C1, is used in comparison with both the analytical model and FEM simulations. The exception is due to the lack of tabulated data for this alloy-treatment group.

Extrusion Tests. The extrusion tests were performed on an 800-ton hydraulic laboratory extrusion press as reported in [5, 20]. The billets were induction heated at the press, with a heating rate of about 80 °C per minute to different pre-heating temperatures without any taper. The container diameter was 100 mm and the container temperature was kept at 430 °C for all experiments. In order to measure the critical temperature when surface defects appear during extrusion, thermocouples were inserted into the bearing surface of the extrusion die protruding 0.1 mm into the surface of the extruded rod [5, 20]. The profile was a solid rod with diameter of 9 mm and the die consisted of a 3 mm and 1-degree chocked region, and a 1 mm parallel bearing surface. The profiles were water quenched about three meters from the die.

Table 1. Chemical composition (wt%) of the alloys used in the present investigation [5, 20].

Alloy	Mg	Si	Fe	Mn	Cr	Cu
A	0.58	0.91	0.20	-	-	-
C	0.60	0.92	0.22	0.52	-	-
D	0.58	0.93	0.21	-	0.15	-
E	0.61	0.94	0.20	0.53	0.15	-
F	0.60	0.95	0.21	0.53	0.14	0.10
G	0.60	1.26	0.21	0.56	-	-
H	0.80	0.92	0.20	0.54	-	-
I	0.85	1.26	0.22	0.56	-	-

Table 2. Input parameters used in analytical temperature model.

Parameter	Unit	Value	Comment
α_d	degrees	45	Chosen value for the semi-die angle
β	-	0.95	Typical value for efficiency factor [1]
c	J (kg K)$^{-1}$	900	Specific heat capacity of alloy in billet (estimated)
c_c	J (kg K)$^{-1}$	490	Specific heat capacity of container alloy (steel) [1]
C	s^{-1}	7.0 x 10^8	Material constant in Eq. 3, [6,10]
D_c	m	0.100	Container diameter
D_e	m	0.009	Extrusion diameter (rod shaped extrusion)
k_{ss}	MPa (wt%)$^{-3/4}$	3.0	Material constant in Eq. 6, [6,10]
k_d	MPa (m^{-1})	4.8	Material constant in Eq. 7, [6,10]
k_4	-	0.55	Constant in Eq. 13
k_5	Kms(N)$^{-1}$	8.0 x 10^{-8}	Constant in Eq. 17
λ	W (mK)$^{-1}$	150	Thermal conductivity of alloy in billet (estimated)
λ_c	W (mK)$^{-1}$	32.7	Thermal conductivity of container alloy (steel) [1]
L_b	m	0.20	Billet length
L_d	m	0.001	Die bearing length
n	-	5.0	Material constant in Eq. 3, [6,10]
Q_{app}	J (mol)$^{-1}$	156000	Apparent activation energy [6,10]
ρ	kg (m^{-3})	2700	Density of alloy in billet (estimated)
ρ_c	kg (m^{-3})	7860	Density of container alloy (steel) [1]
R_g	J (K mol)$^{-1}$	8.314	Universal gas constant
T_c^0	°C (or K)	430 (703)	Initial container temperature

Results and Discussion

In the following section, results using the modelling framework described above are presented and compared with experimental data from the extrusion trials for the solid bar profile reported in [20].

Input Data. The analytical temperature model requires a wide spectrum of input data before a prediction can be made. These are summarised in Table 2. Both the FEM model as well as the analytical temperature model require input data for the deformation resistance as expressed by the parameters σ_{ss} and σ_d . These parameters have been predicted by the microstructure-based model Alstruc [7,8] for the various alloys and homogenisation cycles in the present investigation, and the values are given in Table 3. The table also includes measured temperatures for incipient surface tearing T_c for the different alloys from [20].

Table 3. Measured temperature for incipient surface tearing T_c for the different alloys [20] and predicted hot-deformation parameters σ_{ss} and σ_d from Alstruc [7,8]. (The critical temperature was not obtained for alloy C1).

Alloy	**A1**	**A2**	**C1**	**C2**	**D1**	**D2**	**E1**	**E2**
T_c **(°C)**	575	571	-	587	583	583	593	594
σ_{ss} **(MPa)**	16.81	16.57	17.17	16.91	17.50	17.50	17.20	16.94
σ_d **(MPa)**	0.52	1.84	3.64	7.53	1.29	1.58	3.69	9.25
Alloy	**F1**	**F2**	**G1**	**G2**	**H1**	**H2**	**I1**	**I2**
T_c **(°C)**	591	591	560	565	588	588	579	584
σ_{ss} **(MPa)**	17.50	17.50	17.50	17.50	17.50	17.50	17.70	17.50
σ_d **(MPa)**	3.51	9.28	4.51	7.56	3.77	7.13	4.27	7.36

Temperatures from FEM-simulations Figure 1 (b) shows a typical example of outputs from a finite element simulation, visualising contour plots of the temperature distribution in the billet and the rod during extrusion. Figure 1 (a) shows the flow domain as the material exits the die through the choked area before flowing across the parallel bearing surface.

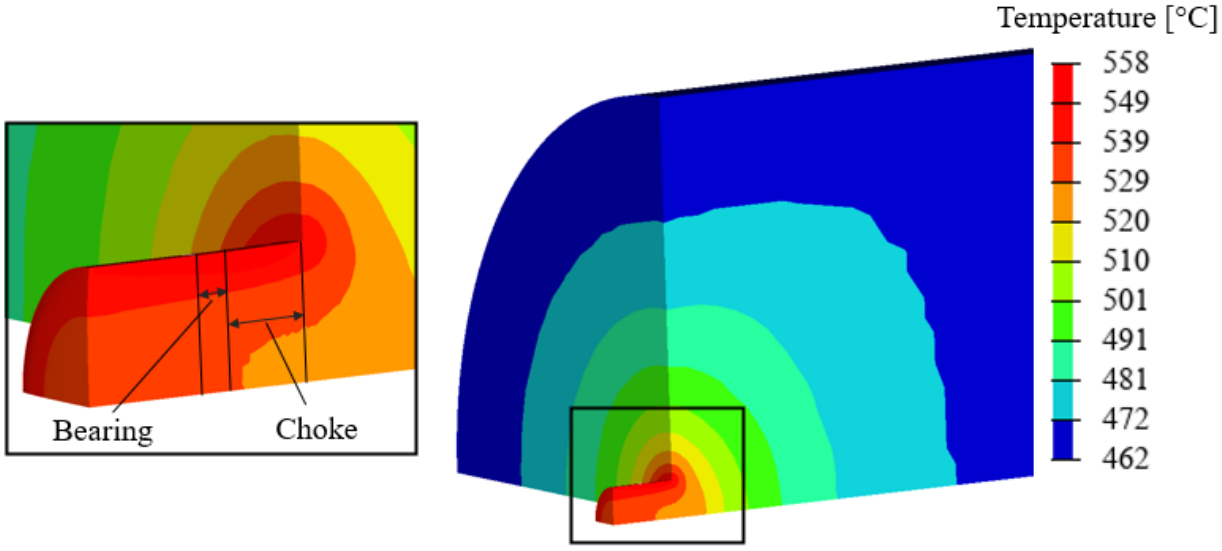

Fig. 1. Example of outputs from the finite element simulations. (a) and (b) shows the contour plot of the temperature distribution during extrusion of alloy A1, applying a ram speed of v_r= 7.0 mm/s and an initial billet temperature of T_0 = 462 °C. (b) bearing and choke region of the flow domain.

Flow Patterns Figure 2 shows the corresponding flow pattern for the simulation presented in Figure 1. The dead metal zone is visible as a volume with little to no material flow in the extrusion direction, located near the end of the container. The semi-die angle α_d which is used as input to the analytical model, is superimposed in Figure 2 (a). It is evident from this figure that α_d is not clearly defined, as the flow patterns are curved. However, it seems reasonable to use values in the range 30-60 degrees in the analytical solution, and a value of 45 degrees was selected in the present work.

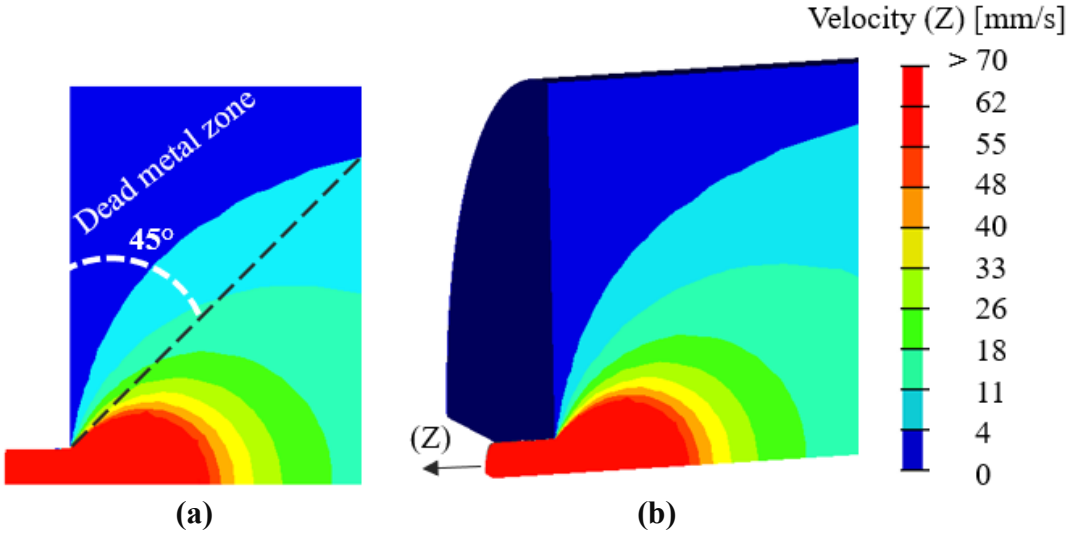

Fig. 2. Simulation of material flow in the extrusion direction near the end of the container evaluated for alloy A1 applying a ram speed of v_r= 7.0 mm/s and an initial billet temperature of T_0 = 462 °C. (a) 2D cross section with the superimposed semi-die angle α_d=45° used in the analytical model. (b) 3D contour plot of the material flow in the extrusion direction shown for the quarter model.

Temperature Contributions in Analytical Model. In Figure 3, the temperature contributions ΔT_1, ΔT_2, ΔT_3, ΔT_4, and ΔT_5 as predicted by the analytical model, are plotted as a function of the ram speed for alloy A1. The Figure show results for the experimental data grouped by three different

initial billet temperatures, i.e. 420, 460, and 500 °C, respectively. Each figure also shows the sum of these contributions, and a comparison with corresponding measured temperature increase, i.e. the measured exit temperature minus the initial billet temperature. It is evident that the sum of the contributions agrees well with the measured temperature increase for all billet temperatures, although the model seems to underestimate the temperature increase for the initial billet temperatures of 420 °C in Figure 3(a).

A closer inspection of Figure 3 reveals that adiabatic heating, ΔT_1, yields the largest temperature contribution for all combinations of billet temperature and ram speed. The figure also shows that the contribution from redundant work ΔT_5 is the second largest positive contribution. This contribution also shows a stronger dependency on the ram speed than the other contributions in Figure 3. This is not surprising since ΔT_5 is proportional to v_r according to Eq. 17.

The friction-based contributions ΔT_2 and ΔT_3 show similar dependencies with the ram speed, and their magnitude are also in the same range. The expressions in Eq. 9a and Eq. 10, yield ΔT_2 and ΔT_3 proportional to $\sqrt{v_e L_d}$ and $\sqrt{v_r L_b}$, respectively, when $k_2=k_3$, as assumed in this work. Since $v_e=Rv_r$, it follows that the difference between the two contributions can be expressed as $\sqrt{(RL_d)/L_b} = 0.78$ when Eq. 9a applies, which is the case in the present examples. Hence, $\Delta T_2=0.78\ \Delta T_3$, as observed in Figure 3.

The contribution accounting for heat conduction in container and billet, i.e. ΔT_4 can be positive or negative, depending on whether the container temperature is higher or lower than the initial billet temperature. In Figure 3(a), ΔT_4 is small but positive which means a weak heating of the billet. This is because the initial billet temperature is 420 °C which is slightly lower than the container temperature of 430 °C. In Figure 3(b) and 3(c) ΔT_4 is negative since the container temperature is lower than the billet temperature.

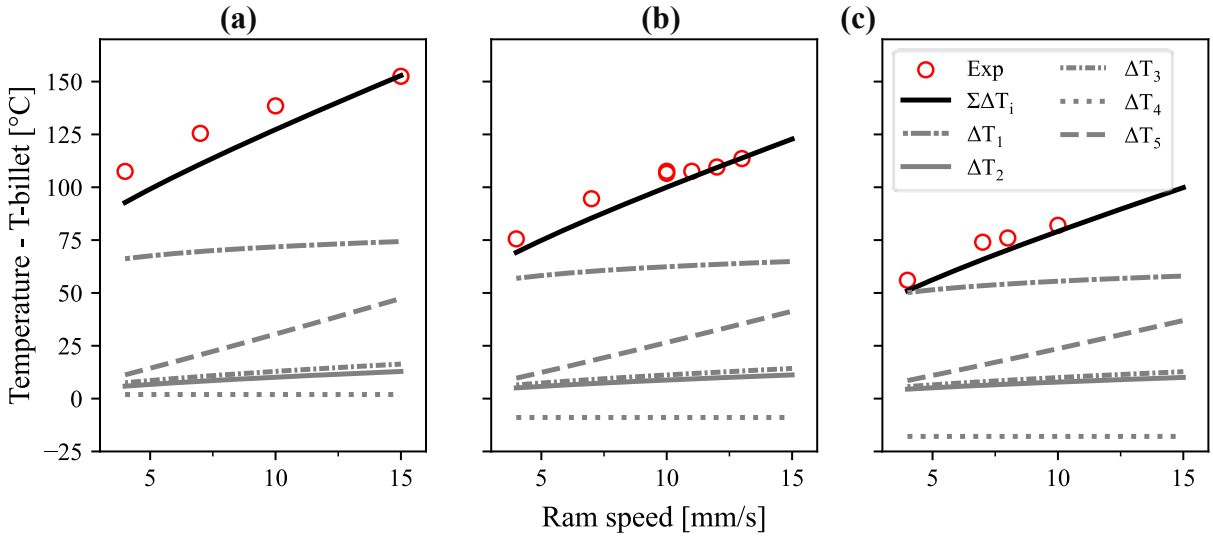

Fig. 3. The contributions to the profile surface temperature at the die outlet position, and the overall temperature increase compared with measurements for alloy A1. (a) billet temperature 420ºC. (b) billet temperature 460ºC. (c) billet temperature 500ºC.

Overall Agreement Between Calculated and Measured Temperatures The described modelling framework was applied to calculate the exit temperatures for all tested combinations of alloy and homogenisation conditions, except C1. Figure 4 (a) shows the overall agreement between measured and calculated temperatures for FEM simulations, and the same comparison is done for the analytical model in Figure 4 (b). Measured and calculated temperatures are grouped by alloy and homogenisation condition. A closer inspection reveals that each alloy and homogenisation combination, e.g. A1 shows three groups of temperatures, corresponding to three different billet temperatures. In each group, the temperatures increase up to a maximum, and then drops suddenly. The temperature increase corresponds to increasing ram speed at constant billet temperature, while

the sudden drop, corresponds to transition from one billet temperature to another. The results in Figure 4 and the deviation between measured and predicted data are collected in scatter plots in Figure 5.

From these diagrams, it is evident both the numerical model and the analytical temperature model provide quite accurate predictions of the measured temperatures. Hence the maximum absolute value of the deviation between calculated and measured temperatures is 16.2 °C for the FEM model, while the standard deviation is 7.0 °C. The corresponding values for the analytical temperature model are 20.8 °C, and 8.0 °C, respectively. Hence, the analytical model gives slightly less accurate predictions than the FEM model for the present alloys, which is to be expected when considering the difference in complexity between the models.

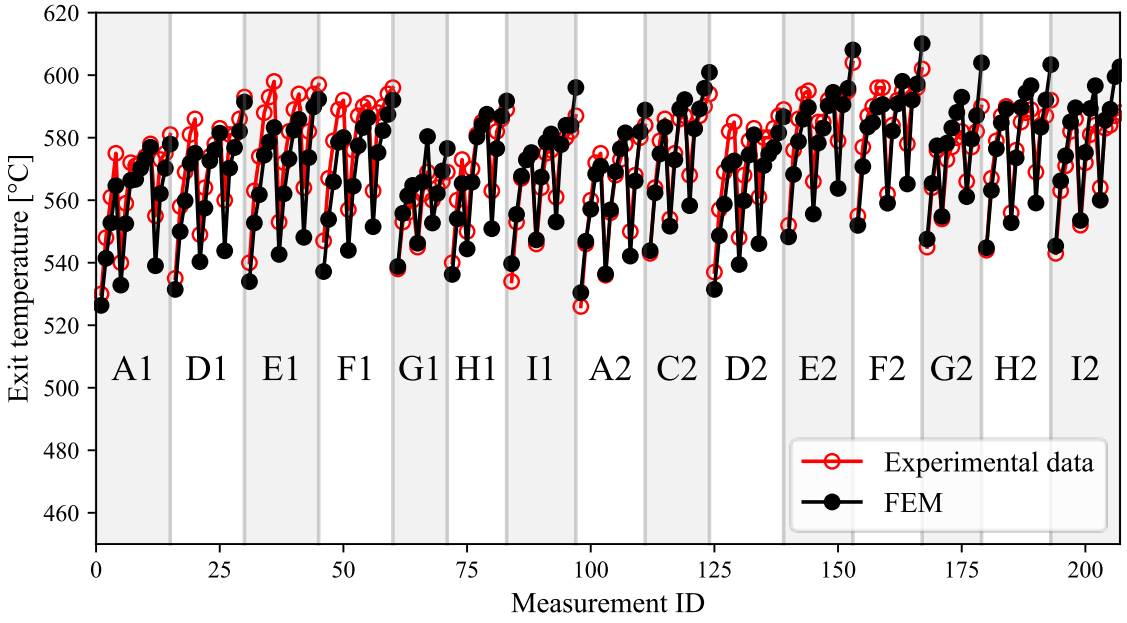

(a)

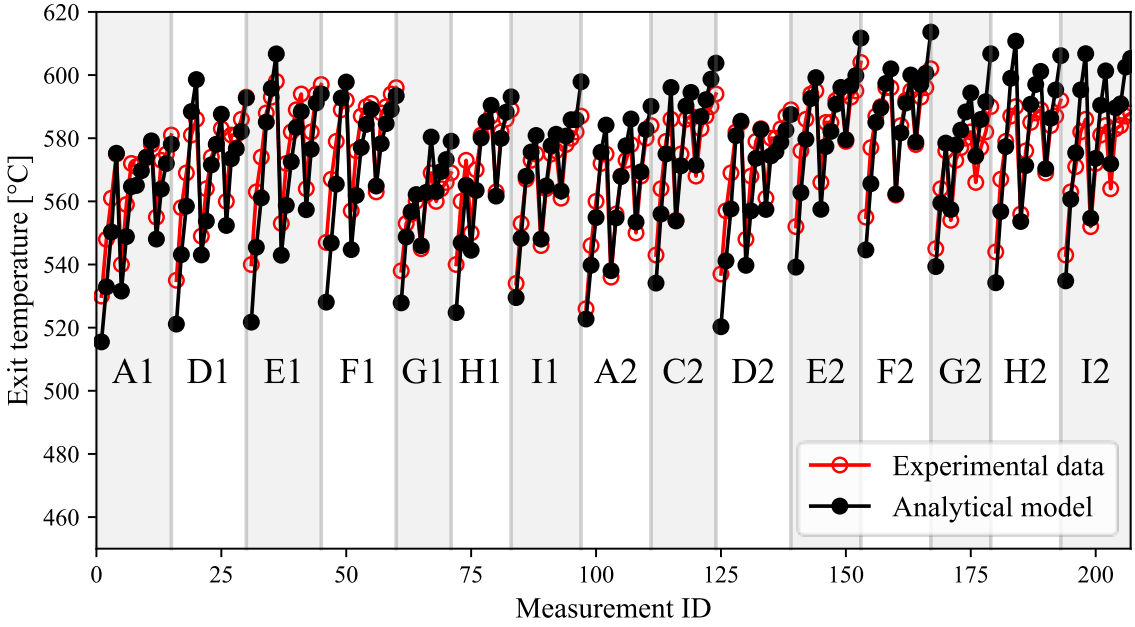

(b)

Fig. 4. Comparison between the predicted and measured temperatures at the die outlet position for all alloy compositions and homogenisation treatment groups, except C1. (a) Predictions made by the FEM model compared to measured temperatures, grouped by alloy and homogenisation treatment. (b) Predictions made by the analytical model compared to measured temperatures, grouped by alloy and homogenisation treatment.

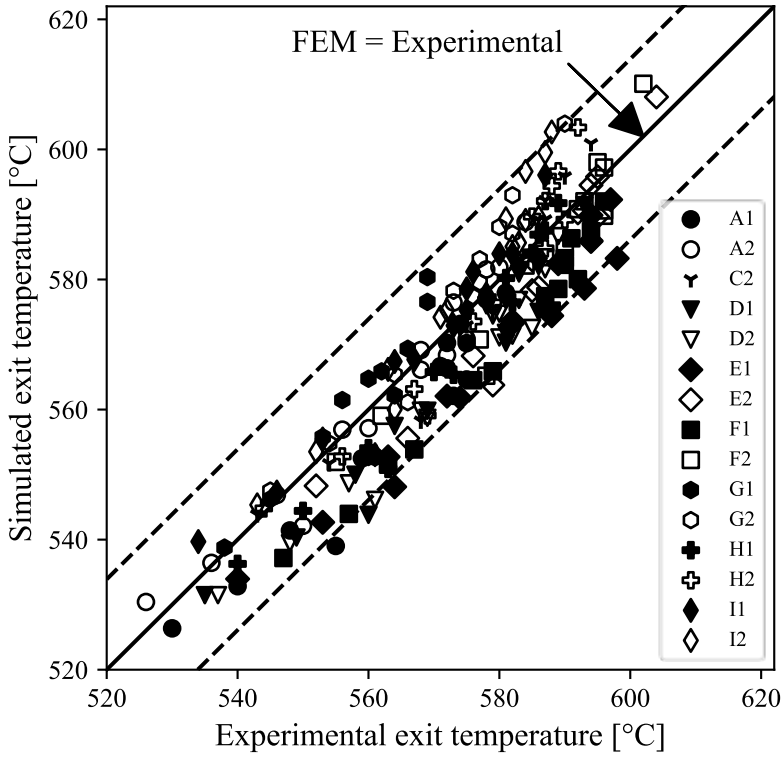

(a)

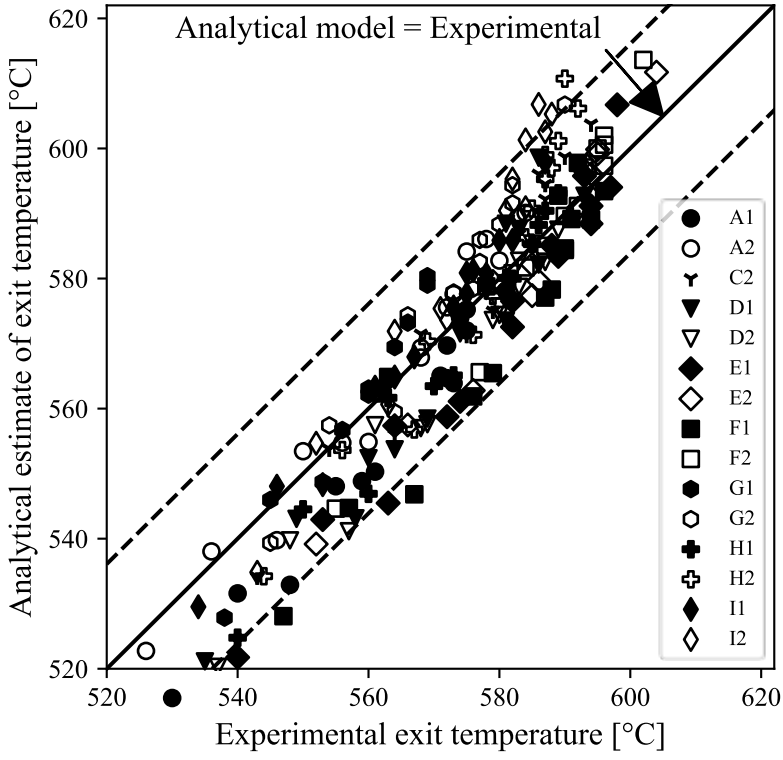

(b)

Fig. 5. Comparison of the deviation between the predicted and measured temperatures at the die outlet position. (a) Scatter plot of FEM predictions vs. measured temperatures. (b) Scatter plot of analytical predictions vs. measured temperatures. In both (a) and (b) the fully drawn line indicates a one-to-one relation between experimentally obtained results and predicted temperatures. The dashed line indicates the one-to-one relation +/- two times the standard deviation calculated for the total deviation between measured and predicted exit temperatures.

Extrusion Limit Diagrams The predicted surface temperatures from the previous section were used to construct extrusion limit diagrams which are plots of the maximum allowable ram speed with respect to surface tearing as a function of billet preheat temperature. Such diagrams require that the critical temperature, above which hot tearing appears, is known. In the present work, the critical temperature for each alloy was obtained from measured temperatures at the profile surface combined with visual inspection of the surface at the die outlet during extrusion tests as described in [20]. In the tests, the profile surface was classified in three groups, i.e., no tearing, incipient tearing, or tearing. By analysing the data, critical temperatures T_c for the transition from "no tearing" to "tearing" for each alloy, given in Table 2, were estimated. These temperatures, and the predicted deformation resistance parameters for each alloy in Table 2 were used as inputs to the analytical temperature model to calculate the resulting temperature at the die outlet as a function of billet temperature and ram speed. The resulting extrusion limit diagrams are shown as solid lines in Figure 6. The scattered data in Figure 6 show the experimental surface characterisation from the extrusion trials described in [20].

The calculated extrusion limit curves in Fig. 6 are generally in good agreement with the experimental results represented by the symbols. The model seems to capture the observed effect of alloy composition and homogenisation cycle on the resulting extrusion limits. Hence, alloys with low deformation resistance allow higher ram speeds than alloys with high deformation resistance. This can be seen by comparing for instance alloy A1 and F2 for a billet temperature of 400 °C, where the critical ram speeds are 15.9 mm/s and 12.0 mm/s, respectively. The reason for higher ram speed for A1 compared with F2 is because the deformation resistance parameters σ_{ss} and σ_d are lower for A1 than for F2, as can be seen from Table 2.

There is also an effect of critical temperatures T_c for the transition from "no tearing" to "tearing" for each alloy, which is alloy dependent and therefore affects the diagrams in Fig. 6. The higher T_c, the higher ram speed can be applied. This is the reason why for instance alloy E2, which has a high deformation resistance in terms of σ_{ss} and σ_d values, still can be extruded with relatively high ram speeds according to Fig. 6. This is because T_c for alloy E2 is 594 °C, which is the highest T_c temperature in Table 2. Hence, it is the combination of σ_{ss}, σ_d, and T_c that give the resulting extrusion limitation curves, and low σ_{ss} and σ_d values in combination with high T_c values are all positive in order to displace the extrusion limitation curves to higher values.

Since the predicted extrusion limit curves in Fig. 6 are significantly influenced by the estimated T_c temperatures, it follows that the accuracy of the predicted temperatures at the die exit are also crucial for realistic results when applying the diagrams. Hence, relatively small inaccuracies in the prediction of the die exit temperature, may give serious inaccuracies in the predicted extrusion limitation curves. This is shown in Fig. 7, where the various curves represent different deviations from the predicted profile exit temperatures for alloy A1 from Fig. 6. It follows from this diagram that an inaccuracy of +/- 5 °C in the predicted exit temperature, yields a corresponding inaccuracy of about +/- 1mm/s.

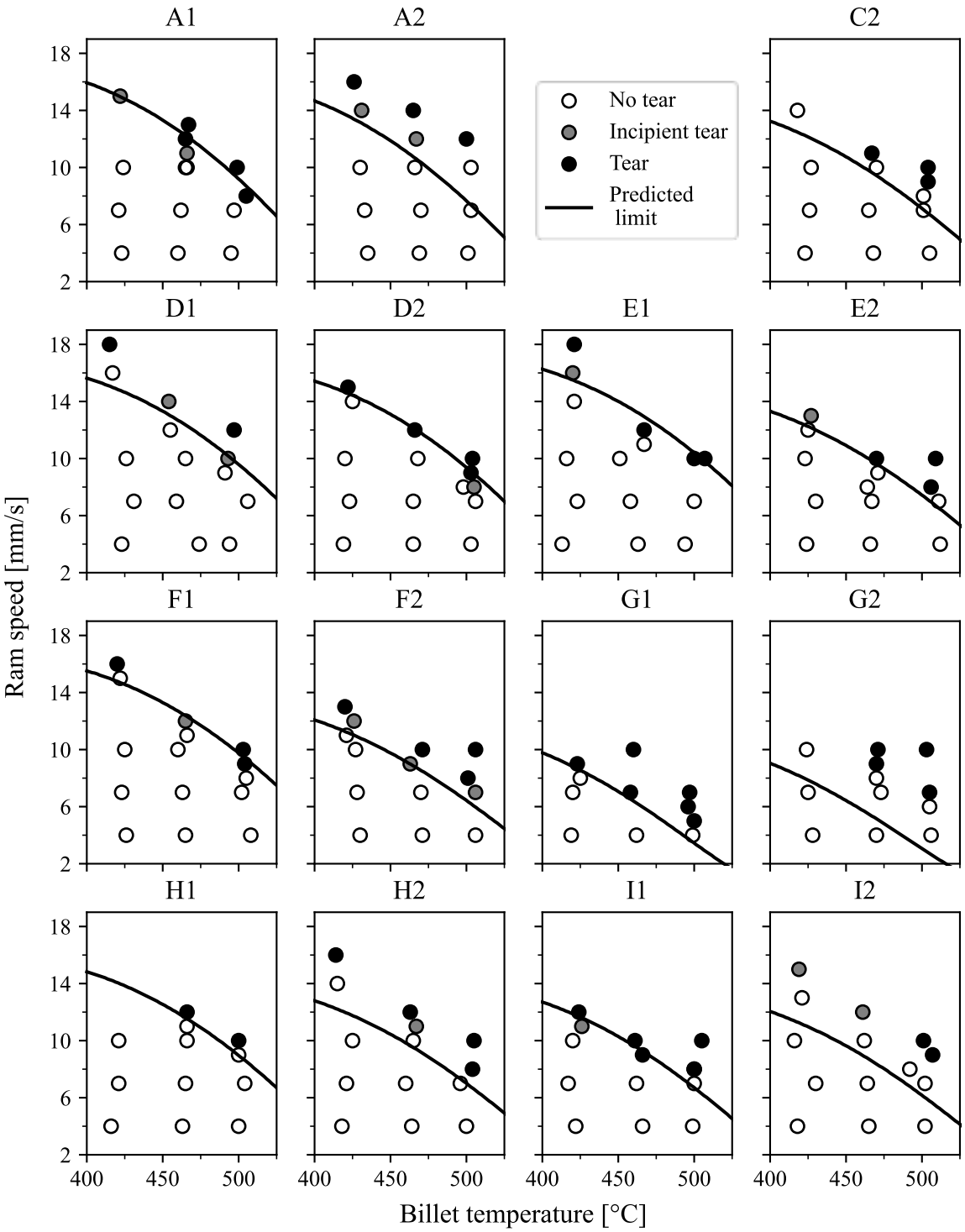

Fig. 6. Experimental distribution of surface tearing data for all alloy-treatment groups, except C1, compared to predicted extrusion limit. The experimental data are grouped by alloy composition and homogenisation treatment and redrawn from [20]. For each alloy-treatment group, open circles indicate a surface without hot tearing defects, partially filled circles indicate incipient hot tearing, and fully filled circles indicate hot tearing. Solid line shows the predicted extrusion limit diagrams applying the analytical exit temperature model.

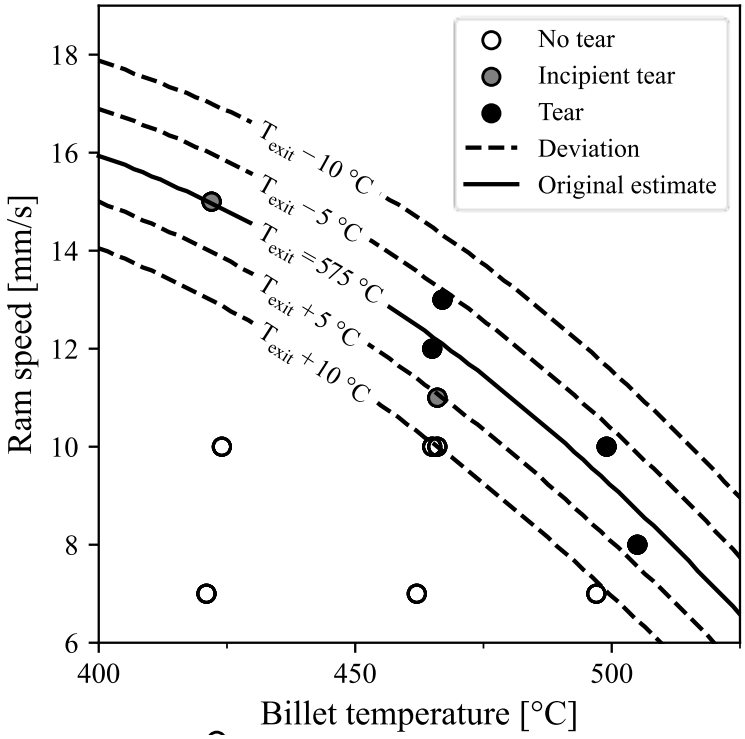

Fig. 7. Effect of deviation in surface exit temperature on resulting extrusion limitation curves, visualised for alloy composition and homogenisation group A1. Solid line indicates the original extrusion limit prediction, as shown for A1 in Figure 6. In increments of 5 °C, the dashed lines show how temperature deviations in the analytically calculated exit temperature affects the prediction of the extrusion limit curve.

Conclusions

The main conclusions that can be drawn from this investigation are as follows:

1. A comparison between predicted and measured temperatures at the die exit shows that the presented analytical model is reasonably accurate compared with FEM simulations for the present profile geometry. Hence, standard deviations of 7.0 °C and 8.0 °C were obtained for the FEM model and the analytical temperature model, respectively, while the maximum absolute value of the deviation between calculated and measured temperatures was 16.2 °C for the FEM model and 20.8 °C for the analytical temperature model.
2. Both the analytical model and the FEM simulations capture the observed effect of alloy composition and homogenisation heat treatment on the resulting temperatures. This is because both models incorporate the effect of processing and alloy composition in the constitutive equations for the deformation resistance.
3. A comparison between calculated extrusion limit diagrams using the analytical temperature model, and results from real extrusion tests shows good correlations for the different alloys and homogenisation heat treatments applied.
4. A sensitivity analysis performed for one of the alloys in this investigation reveals that the predicted extrusion limit diagrams are sensitive to variations in the predicted exit temperature. Hence, an inaccuracy of +/- 5 °C in the predicted exit temperature, yields a corresponding inaccuracy of +/- 1 mm/s in the diagrams for the investigated alloy.
5. Based on the results in this investigation, it is concluded that the presented modelling approach gives sufficiently accurate predictions for future application in optimisation of process parameters in extrusion of profiles in the 6xxx series aluminium alloys.

Future Work

Future work will be focused on extending the analytical modelling approach to more complex profile cross sections including hollow profiles. Work is also in progress to couple the critical temperature for incipient surface tearing to temperatures that can be estimated from multi-component phase diagrams using various types of microstructure-based models like the Alstruc-model that has been briefly described in the present article.

References

[1] T. Sheppard, in: Extrusion of Aluminium Alloys, Springer, New York, NY (1999).

[2] O. Reiso: *The effect of Billet Preheating Practice on Extrudability of AlMgSi Alloys* (Proceedings of the 4th. International Aluminium Extrusion Technology Seminar, Aluminium Association, USA 1988)

[3] O. Reiso: *The Occurrence of Surface Defects during Extrusion from a Metallurgical Point of View* (Deutche Gesellshaft fur Materialkunde, Germany 1990)

[4] HyperXtrude®, Altair Engineering Inc.

[5] J. Røyset, M. Marstrander Rødland, U. Tundal, and O. Reiso: *Effect of Alloy Chemistry and Process Parameters on the Extrudability and Recrystallization Resistance of 6082 Aluminum Alloy* (Proceedings of the Ninth International Aluminum Extrusion Technology Seminar, Extrusion Technology for Aluminum Profiles Foundation, USA 2008)

[6] T. Furu, N. Telioui, R. Østhus, R. Aagård, M. Bru, and O. R. Myhr: *The effect of Mn on Extrudability, Mechanical Properties and Grain Structure of 6082 Alloys* (Proceedings of the Eleventh International Aluminum Extrusion Technology Seminar, Extrusion Technology for Aluminum Profiles Foundation, USA 2016)

[7] A. L. Dons: Journal of Light Metals, Vol. 1 (2001), p. 133.

[8] A. L. Dons, E. K. Jensen, Y. Langsrud, E. Trømborg and S. Brusethaug: Metallurgical and Materials Transactions, Vol. 30A (1999), p. 2135.

[9] O. Reiso: *The Effect of Microstructure on the Extrudability of Some Aluminium alloys* (Doctorial thesis, Norwegian University of Science and Technology, Norway 1992)

[10] O. R. Myhr, R. Østhus, A. Nesse, and T. Furu: *Modelling of Recrystallization, Quench Sensitivity and Surface Tearing of 6xxx Alloys* (Proceedings of the Twelfth International Aluminum Extrusion Technology Seminar, Extrusion Technology for Aluminum Profiles Foundation, USA 2022)

[11] H. P. Stuwe: Metall, Vol. 22 (1968), p. 1197.

[12] A. Jackson, T. Sheppard: Materials Science and Technology. Vol. 13 (1997), p. 61.

[13] M. Bauser, G. Sauer, K.Siegert, in: *Extrusion*, Second Edition, ASM International, Materials Park, Ohio (2006).

[14] S. Støren, P.T. Moe, in: *Handbook of Aluminium*, Vol. 1, Marcel Dekker, Inc., New York, Basel, (2003)

[15] G. E. Dieter, in: *Mechanical Metallurgy*, McGraw-Hill Book Company, New York, NY (1986).

[16] P. Feltham: Metal Treatment, Vol. 23 (1956), p. 440.

[17] S. Abtahi: *Friction and interface reactions on the die land in thin-walled extrusion* (Doctorial thesis, Norwegian University of Science and Technology, Norway 1995)

[18] T. L. Bergman, A. Lavine, F.P Incropera, and D. P. Dewitt, in: *Fundamentals of Heat and Mass transfer*, John Wiley & Sons, Hoboken, NJ (2011).

[19] P. K. Saha, in: *Aluminium Extrusion Technology*, ASM International, Materials Park, Ohio (2000).

[20] U. Tundal, O. Reiso: *Aluminium report 95-29/3-40* (Hydro, Norway 1995).